HMG Advance Access published May 23, 2011

Human Molecular Genetics, 2011 **1–14**
doi:10.1093/hmg/ddr203

Neuron-specific proteotoxicity of mutant ataxin-3 in *C. elegans*: rescue by the DAF-16 and HSF-1 pathways

Andreia Teixeira-Castro[1,2], Michael Ailion[3], Ana Jalles[1], Heather R. Brignull[2,†], João L. Vilaça[1,4], Nuno Dias[1,4], Pedro Rodrigues[1], João F. Oliveira[1], Andreia Neves-Carvalho[1], Richard I. Morimoto[2,‡] and Patrícia Maciel[1,*,‡]

[1]Life and Health Sciences Research Institute (ICVS), School of Health Sciences, University of Minho, Campus de Gualtar, 4710-057 Braga, Portugal, [2]Department of Molecular Biosciences, Northwestern University Institute for Neuroscience, Rice Institute for Biomedical Research, Northwestern University, Evanston, IL 60208, [3]Department of Biology, University of Utah, Salt Lake City, UT 84112, USA and [4]DIGARC, Polytechnic Institute of Cávado and Ave, 4750-810 Barcelos, Portugal

Received February 23, 2011; Revised and Accepted May 1, 2011

The risk of developing neurodegenerative diseases increases with age. Although many of the molecular pathways regulating proteotoxic stress and longevity are well characterized, their contribution to disease susceptibility remains unclear. In this study, we describe a new *Caenorhabditis elegans* model of Machado–Joseph disease pathogenesis. Pan-neuronal expression of mutant ATXN3 leads to a polyQ-length dependent, neuron subtype-specific aggregation and neuronal dysfunction. Analysis of different neurons revealed a pattern of dorsal nerve cord and sensory neuron susceptibility to mutant ataxin-3 that was distinct from the aggregation and toxicity profiles of polyQ-alone proteins. This reveals that the sequences flanking the polyQ-stretch in ATXN3 have a dominant influence on cell-intrinsic neuronal factors that modulate polyQ-mediated pathogenesis. Aging influences the ATXN3 phenotypes which can be suppressed by the downregulation of the insulin/insulin growth factor-1-like signaling pathway and activation of heat shock factor-1.

INTRODUCTION

Machado–Joseph disease (MJD) (or spinocerebellar ataxia type 3) is the most common dominantly inherited ataxia worldwide (1,2). This adult-onset neurodegenerative disorder is characterized by ataxia, ophthalmoplegia and pyramidal signs, associated in variable degree with dystonia, spasticity, peripheral neuropathy and amyotrophy (3), but with no cognitive decline. Pathologically, the disorder is associated with the degeneration of the deep nuclei of the cerebellum, pontine and subthalamic nuclei, substantia nigra and spinocerebellar nuclei. Similar to Huntington's disease (HD), spinobulbar muscular atrophy and other ataxias, MJD is caused by a translated unstable CAG trinucleotide-repeat expansion. The resulting polyglutamine (polyQ) expansions render the affected proteins susceptible to abnormal conformations that promote the formation of neuronal inclusions (4–6). Despite this unifying feature, specific populations of neurons are affected in different polyQ disorders, suggesting that protein domains outside the polyQ tract contribute to the pathological signature of each disease. In MJD, it is known that this neuron-specific susceptibility is not the result of the mutant ataxin-3 (ATXN3) expression pattern, as this protein, like all the other polyQ-containing proteins, is widely expressed from very early stages of development (7,8). ATXN3 is a small protein that contains a cysteine protease-like domain, the Josephin domain and two or three ubiquitin-interacting motifs (UIMs). Among the polyQ-containing proteins, ATXN3 is

*To whom correspondence should be addressed at: Life and Health Sciences Research Institute (ICVS), School of Health Sciences, University of Minho, Campus de Gualtar, 4710-057 Braga, Portugal. Tel: +351 253604824; Fax: +351 253604820; Email: pmaciel@ecsaude.uminho.pt
†Present address: Department of Biological Structure, University of Washington, Seattle, WA 98915, USA.
‡Research was shared equally among the two laboratories.

unique because it has been implicated in cellular protein degradation pathways, through its deubiquitylase (9–12) and deneddylase (13) activities.

The mean age at onset of MJD is 37 years (14) and correlates significantly with the number of CAG/polyQ repeats, with earlier onset in individuals with larger repeat sizes. However, there is considerable individual variation of age at onset within a given repeat-length range (reviewed in 15, highlighting the role of other genetic and environmental factors. Correlative evidence suggests aging as a major risk factor for the development of many neurodegenerative diseases (16). Typically, individuals that carry neurodegeneration-linked mutations develop the disease during their fifth decade, whereas sporadic cases appear during the seventh decade or later (17). It is still unclear why distinct neurodegenerative diseases occur late in life with overlapping temporal inceptions. One likely possibility is that the aging process interferes with the cellular proteostasis machinery, enabling misfolding, aggregation and initiating neurodegeneration (18,19). Recent studies point to the insulin/insulin growth factor (IGF)-1-like signaling (IIS) pathway, facilitated by heat shock factor-1 (HSF-1), as major candidates that link aging, proteotoxicity and neurodegenerative diseases (20–22).

MJD pathogenesis has been recapitulated *in vivo* in a variety of invertebrate and rodent model systems (23–29). *Caenorhabditis elegans* has been successfully used to model neurodegeneration *in vivo*, mainly due to the conservation of basic cellular mechanisms, such as those coupled with neuronal signaling, cell death/survival and the maintenance of proteostasis and aging. The morphology of all 302 neurons has been defined by electron microscopy, and much is known about their synaptic connectivity and functional properties (30,31). Despite having relatively few neurons, *C. elegans* exhibit complex behaviors that can be assayed to monitor neuronal dysfunction, which can be combined with biophysical assays to examine protein solubility in neurons of interest (32). Previous studies using *C. elegans* to investigate polyQ pathology, in subsets of neurons or in body-wall muscle cells, have found a polyQ length-dependent aggregation and toxicity (33–36). Recent studies have introduced the possibility of studying the impact of the expression of a single species of a misfolded polyQ protein on the *C. elegans* nervous system and its toxic behavioral outcome. These studies have shown neuronal subtype-specific vulnerability to the expression of polyQ segments at the threshold Q-length for aggregation and neuronal dysfunction (32).

Here, we have established a new *C. elegans* model of MJD in which ataxin-3 was expressed throughout the nervous system. The comparison of these ATXN3 models with the previously characterized polyQ-alone models (32) should also shed light on the modulatory effects of protein context in pathogenesis. In our model, the expression of both full-length and truncated forms of ataxin-3, with different Q-lengths, results in a consistent pattern of neuronal cell-type-specific aggregation, with the ventral and dorsal nerve-cord neurons being highly affected, while some lateral interneuron cell bodies are resistant. Certain sensory processes in the head contain aggregated foci, but only when the polyQ stretch is within the ATXN3 protein-flanking sequences, and not when expressed alone. We have also studied the impact of aging and of reprogramming animals' survival in our model, and we found that reducing IIS and activating HSF-1 pathways (genetically or pharmacologically) reduced pathogenesis, supporting the mechanistic links between the aging process and neuronal toxic-protein aggregation, which are common hallmarks of many neurodegenerative disorders.

RESULTS

Expression of full-length ataxin-3 in live neuronal cells causes polyQ length-dependent aggregation

The pathogenesis of ATXN3 was studied in transgenic *C. elegans* strains expressing human wild-type (WT) or pathological full-length ATXN3 throughout the nervous system. Normal-length (q14) and mutant (q75 and q130) ATXN3 were tagged at the C-terminus with YFP and expressed in neuronal cells under the control of the promoter of the *F25B3.3* gene (Supplementary Material, Fig. S1A). This gene encodes a *C. elegans* ortholog of the Ca^{2+}-regulated Ras nucleotide exchange factor, RasGRP, that is expressed widely throughout the nervous system. The *F25B3.3* gene promoter ($P_{F25B3.3}$) becomes active in the comma stage of embryogenesis and expression persists after the terminal division of neurons (37). Expression of YFP-alone (Q0) and Q(*n*)::YFP (Q*n*, $n =$ number of glutamines) under the control of the *F25B3.3* promoter occurs throughout the nervous system (32), demonstrating that $P_{F25B3.3}$ is an appropriate tool to evaluate the response of different neurons to pathological ATXN3.

We verified that the levels of WT or mutant ATXN3 mRNA and protein expressed in transgenic lines were equivalent and at the expected molecular size (Supplementary Material, Fig. S2A and B). Only transgenic lines expressing levels of ATXN3 mutant proteins similar to or lower than the WT ATXN3 were selected for further study, as higher expression levels could influence aggregation and toxicity (Supplementary Material, Fig. S2A).

Analysis of the transgenic animals expressing ATXN3 proteins revealed that pan-neuronal expression of WT AT3q14 resulted in diffuse neuronal distribution (Fig. 1, panel 1), similar to that observed for Q0 animals (32). Uniform diffuse expression of AT3q14 was detected in the nucleus and the cytoplasm of neuronal cell bodies and processes along the entire length of the ventral nerve cord (VNC) (Fig. 1, panel 1, thin arrow) and the dorsal nerve cord (DNC) (Fig. 1, panel 1, thick arrow). Likewise, animals expressing AT3q75 also showed diffuse YFP fluorescence, similar to WT AT3q14 animals in the cell bodies and processes throughout the nervous system (Fig. 1, panel 2). However, AT3q130 animals show heterogeneity with discrete foci detected in some neurons and diffuse protein in other neurons. Foci formation was clearly evident in both the nucleus and the cytoplasm of cell bodies and in neuronal processes of VNC (Fig. 1, panel 3, thin arrow and Supplementary Material, Fig. S3A, C and D, respectively), DNC (Fig. 1, panel 3, thick arrow), commissures (Supplementary Material, Fig. S3B) and certain nerve ring cells (Fig. 1, panel 3, arrow head). AT3q130 foci were observed in the first larval stage

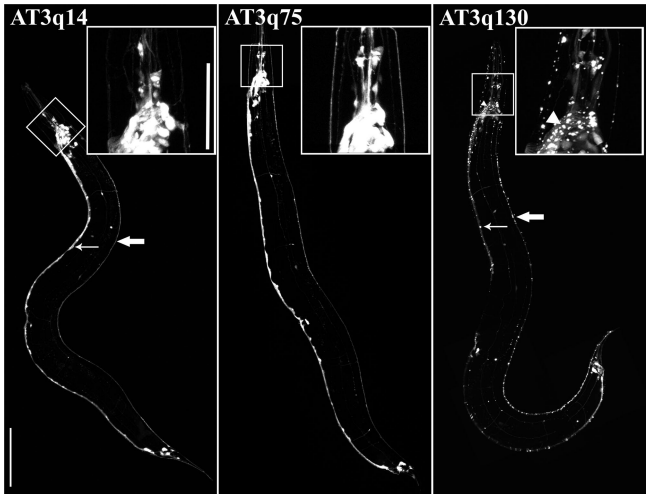

Figure 1. Pan-neuronal expression of full-length ATXN3 in *C. elegans* causes polyQ length-dependent changes in protein distribution. Expression of AT3q14 and AT3q75 proteins displayed a smooth and diffuse distribution pattern (left and middle panels, respectively), whereas AT3q130 proteins are found in discrete foci in certain neurons and are soluble in others (right panel). In the left panel, AT3q14 protein expression could be visualized in cell bodies (thin arrow) and in neuronal processes (thick arrow). In panel 3, the distribution of AT3q130 proteins was strikingly different: foci formation was clearly evident in VNC (thin arrow), DNC (thick arrow) and in certain cells of the circumpharyngeal nerve ring (arrow head). All animals depicted are young adults (4 days post-hatching). Scale bar, 100 μm. White boxes indicate magnified regions. The images were obtained using a Zeiss LSM 510 confocal microscope.

(L1) (Supplementary Material, Fig. S4A) and persisted throughout the lifespan.

We further characterized the AT3q130 foci by dynamic imaging and fluorescence recovery after photobleaching (FRAP) techniques to distinguish between foci of soluble or aggregated protein. As shown in Figure 2, the recovery rate after photobleaching observed for WT ATXN3 (AT3q14) and AT3q75 proteins in neurons was indistinguishable from the soluble Q0 control. In contrast, the AT3q130 foci exhibited only partial recovery (30% recovery over 150 s) [AT3q130 (A)], consistent with the properties of an immobile aggregated species and similar to that observed for the well-characterized Q67::YFP (Q67) aggregates (Fig. 2A and B) (32). We therefore employed the FRAP analysis to examine the foci in discrete neurons located in the head and tail of the animals, as well as in the VNC (adjoining the vulva) and DNC (opposing the vulva). The diffuse AT3q130 expressed in certain VNC, DNC and lateral neurons by comparison showed rapid FRAP recovery indicating that proteins in these neurons [AT3q130(S)] were soluble. Consistent with this, all soluble proteins analyzed by FRAP showed significant recovery rates at the first time point measured (2.27 s) (Fig. 2).

Phenotypic characterization of ATXN3-expressing animals showed that AT3q14 or AT3q75 animals were similar to WT N2 animals for lifespan and movement, whereas AT3q130 animals were lethargic and had slightly reduced lifespan (Supplementary Material, Fig. S5). Nevertheless, AT3q130 animals developed to adulthood and had similar brood sizes (data not shown).

Expression of a C-terminal cleavage fragment of ataxin-3 forms polyQ length-dependent aggregates in *C. elegans* neurons

A common feature of many proteins associated with neurodegenerative disease is proteolytic fragmentation. Likewise, there is evidence to support the proteolysis of ATXN3 in mammalian cells, transgenic mice and MJD brain tissue (25,38–40). To gain additional insight into the biochemical and cell biological properties of truncated ATXN3, we expressed a C-terminal fragment of ATXN3 lacking the amino terminal 257 amino acids of the protein (257cAT3) and retaining the polyQ expansion (q14, q75, q80 and q128) and the UIM3 domain of ATXN3 (Supplementary Material, Fig. S1B) (41). For each of these lines, the neuronal expression of 257cAT3 was at the expected molecular size for mRNA and protein, and at comparable or lower levels than WT controls, indicating that this C-terminal ATXN3 fragment is stably expressed (Supplementary Material, Fig. S2A and B).

In young adult animals (day 4, post-hatching), expression of 257cAT3q14 resulted in a diffuse neuronal pattern, as observed for full-length AT3q14 and YFP-alone expressing animals. However, animals expressing 128 polyQs (257cAT3q128) formed discrete foci throughout different cells of the nervous system (Fig. 3A). These animals were smaller in size and more lethargic than AT3q130 expressing animals and WT controls, yet they developed to the adult stage and had progeny, delayed by 1 day when compared with 257cAT3q14 animals. We then examined transgenic lines expressing intermediate polyQ lengths of 257cAT3q75 and 257cAT3q80 and observed the appearance of some neurons with discrete puncta, whereas in other cells only diffuse protein was detected (Fig. 3A). Protein aggregates were detected in day 2 animals (Supplementary Material, Fig. S4B). The appearance of foci in 257cAT3q75, but not in full-length AT3q75, reveals that the C-terminal truncated protein is more aggregation-prone. Animals expressing 257cAT3q75/80 also exhibited similar rates of development to adulthood as animals expressing full-length AT3q14/75 and WT truncated ATXN3 (257cAT3q14) (data not shown).

The biophysical properties of 257cAT3q75 were compared with 257cAT3q14 using FRAP analysis and showed that 257cAT3q14 exhibited rapid recovery after photobleaching (Fig. 3B), whereas foci in 257cAT3q75 neurons did not recover [Fig. 3B, 257cAT3q75(A)]. We observed heterogeneity among 257cAT3q75 expressing neurons; FRAP analysis of multiple VNC neurons showed differences in 257cAT3q75 protein solubility, ranging from completely soluble [Fig. 3B, 257cAT3q75(S)] to completely insoluble [Fig. 3B, 257cAT3q75(A)]. Molecular heterogeneity was also observed in neurons of the head and tail ganglia of the same animals and from independent transgenic lines (data not shown). By comparison, 257cAT3q128 foci formed immobile aggregates in all neurons tested (Fig. 3B). These results demonstrate that the presence of soluble or aggregated C-terminal ATXN3 protein can vary among different neurons and that this aggregation phenotype is strongly influenced by polyQ length.

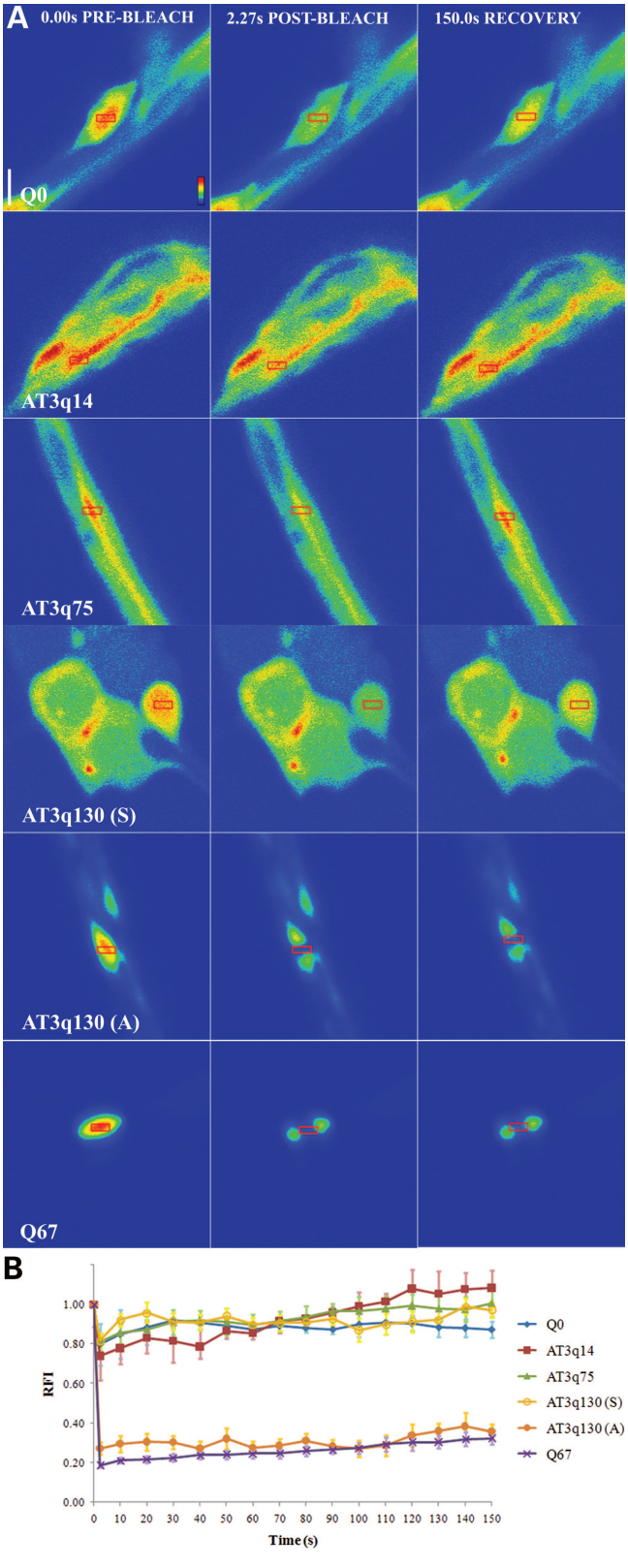

Figure 2. Expression of full-length ATXN3 in live neuronal cells causes polyQ length-dependent aggregation. For FRAP of neurons expressing Q0 proteins, the RFI of the photobleached area (red box), recovers rapidly (**A** and **B** 'Q0'). Similar results were obtained in neurons expressing WT AT3q14 and AT3q75 (A and B 'AT3q14' and 'AT3q75'), indicating the presence of soluble proteins, whereas bleached Q67 foci did not recover (A and B 'Q67'). Q67 proteins are insoluble and were used as an aggregated experimental control. FRAP experiments on AT3q130 animals revealed that some areas display fast FRAP [A and B 'AT3q130 (S)'], whereas others, containing protein foci, did not recover, indicating the presence of a highly immobile aggregated protein [A and B 'AT3q130 (A)']. Quantification (B) was performed in six or more experiments and is represented as the mean ± SEM. Scale bar, 5 μm. The images and FRAP measures were obtained using a Zeiss LSM 510 confocal microscope.

In summary, the aggregation profiles in *C. elegans* neurons for the C-terminal ATXN3 proteins were similar to that observed for the full-length ATXN3 model. The transition from soluble to aggregate states was observed only with the mutant polyQ expansion and exhibited neuron-to-neuron variation. Sequence context also has a role because the expression of 75Qs caused aggregation only in the context of C-terminal ataxin-3 and not of the full-length ATXN3 protein.

Aggregation of mutant ataxin-3 in specific neuronal cells is not stochastic

Previous studies on aggregation of Q40-alone proteins in the nervous system of *C. elegans* showed that aggregation is cell-type-specific and not stochastic, suggesting that polyQ solubility is modulated by the intrinsic properties of the neuronal cell environment (32).

We examined the properties of AT3q130 and 257cAT3q75 in specific neurons of at least two independent transgenic lines. Using the FRAP analysis, both mutant ATXN3 proteins were detected only in a soluble state in HSN neurons (Fig. 4A), whereas in the VNC and DNC neurons both soluble and immobile AT3q130 and 257cAT3q75 were detected (Figs 2 and 3B). Protein aggregates were also detected in certain neuronal processes in the head (Fig. 4B, square), but this occurred only in animals expressing mutant ATXN3-flanking sequences, and not in animals expressing polyQ-alone tracts (32). Many of these processes correspond to sensory neurons. To further examine the expression of mutant ATXN3 in sensory neurons, we co-expressed AT3q130 with mCherry under the regulation of the CHE-13 promoter ($P_{CHE\text{-}13}$::mCherry) that is expressed in nearly all ciliated sensory neurons. Aggregates were not detected in the cell bodies of ASJ, ASI, ADL, ASK, ASE and ASH neurons (data not shown). However, in 88% of the animals analyzed ($N = 50$), CHE-13-positive processes contained aggregated mutant ATXN3 proteins (Fig. 4C). Despite the occasional appearance of aggregates, all six dye-stainable chemosensory amphid neurons in the anterior region (as well as the phasmid tail neurons) exhibited normal DiD staining (data not shown), suggesting that they were functional and not undergoing degeneration.

To confirm that this aggregation pattern was specific rather than stochastic, we co-expressed Q40 (fused to CFP) (32) together with full-length ataxin-3 with polyQ75 (AT3q75) fused to YFP. Whereas AT3q75 does not aggregate in *C. elegans* neuronal cells, co-expression with Q40 resulted in aggregate formation in certain VNC neurons. Analysis of these double-transgenic animals revealed that AT3q75 and Q40 proteins had a synergistic effect in the *C. elegans* nervous

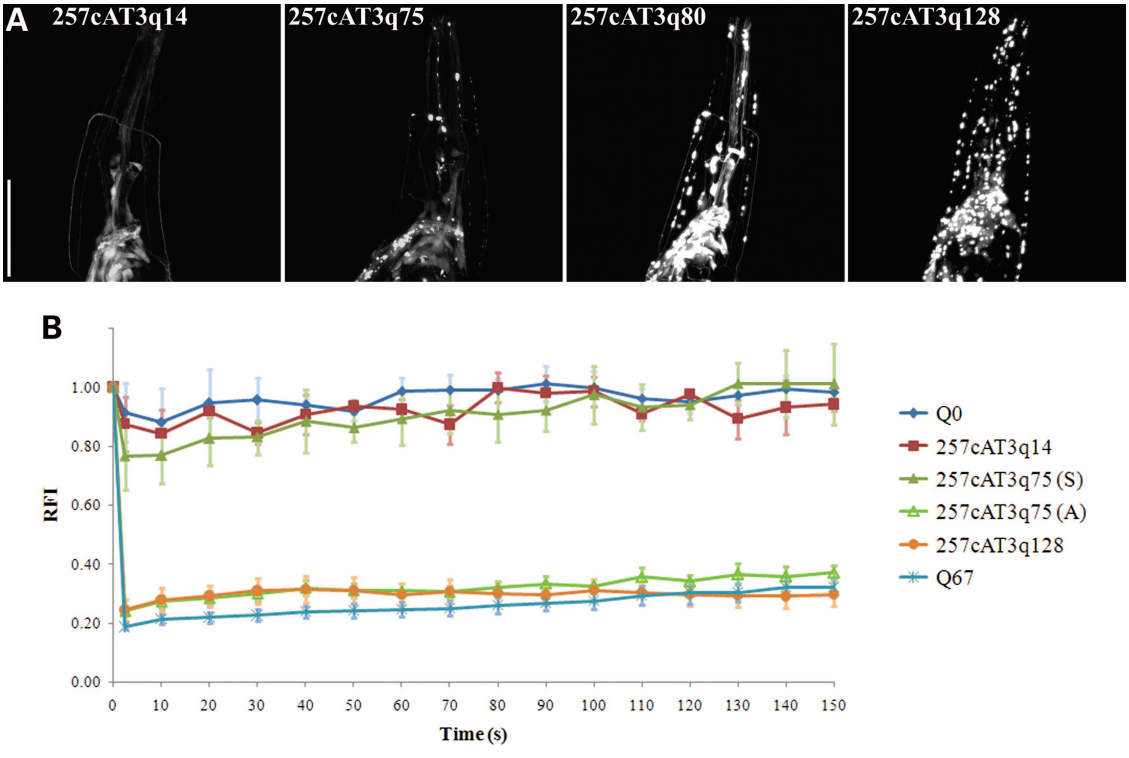

Figure 3. Expression of C-terminal ataxin-3 forms polyQ length-dependent aggregates in *C. elegans* neurons. Flattened z-stacks of *C. elegans* heads revealed that the expression of a range of polyQ lengths within the context of C-terminal ATXN3 flanking regions caused polyQ length-dependent aggregation (**A** and **B**). We observed that 257cAT3q14 proteins displayed a smooth and diffuse distribution pattern, whereas 257cAT3q128 proteins were distributed into discrete foci. The 257cAT3q75 and 257cAT3q80 animals contained protein foci in certain neurons and soluble protein in others (A). Neurons expressing Q0 and 257cAT3q14 proteins recovered rapidly after photobleaching (B, 'Q0' and '257cAT3q14'), indicating the presence of soluble proteins. Bleached Q67 and 257cAT3q128 foci did not recover (B, 'Q67' and '257cAT3q128'). FRAP experiments on 257cAT3q75 animals revealed that some neurons displayed fast FRAP [B, '257cAT3q75 (S)'] whereas others, containing protein foci, did not recover, indicating the presence of insoluble protein (B- '257cAT3q75 (A)'). Quantification (B) was performed in eight or more experiments and is represented as the mean ± SEM. All animals depicted are young adults (4 days post-hatching). Scale bar, 50 μm. The images and FRAP measures were obtained using a Zeiss LSM 510 confocal microscope.

system, as we observed the formation of protein foci in certain processes in the head (Fig. 4D, arrows), but not when either Q40 or AT3q75 proteins were expressed alone, nor when WT AT3q14 and Q40 (Supplementary Material, Fig. S6A) or Q40::CFP and Q40YFP proteins were co-expressed (Supplementary Material, Fig. S6B). Figure 4E shows the quantification of aggregates (42) of the processes of AT3q75;Q40 animals head ($^*P < 0.05$). Even in this example of polyQ synergy, aggregates were not detected in the HSN neurons. These data support a neuron-subtype-specific aggregation pattern in our ATXN3 pathogenesis model that reflects the consequences of ataxin-3 protein context and neuronal cell intrinsic factors.

Ataxin-3 aggregation is highly associated with motor dysfunction

To test whether ataxin-3 expression results in neuronal dysfunction, we performed a series of behavioral assays. Innervation of muscle cells requires more than 60 neurons in *C. elegans* and neuronal dysfunction often results in reduced motility due to a lack of coordination (31,43). In addition to the formation of protein aggregates, expression of mutant ATXN3 (AT3q130) resulted in reduced movement compared with age-matched WT ATXN3-expressing animals (Supplementary Material, Video S1). The motility of the ATXN3-expressing animals was quantified by scoring animals that remained within a 1 cm circle after being transferred into the centre of a freshly seeded plate (44). Animals expressing full-length WT AT3q14 and AT3q75 proteins did not exhibit any impairment at adulthood (day 4), whereas AT3q130 animals exhibited a significant reduction in motility ($^*P < 0.05$) (Fig. 5). In animals expressing the truncated ATXN3, 257cAT3, the effect on motility was even more severe, and we observed a polyQ length-dependent motor dysfunction that correlated with aggregation (Figs 3 and 5). For comparison, we also assessed animals expressing polyQ-alone, and in accordance with what was observed previously, animals expressing Q40 and Q67 had dramatic deficits in motility (32) (Fig. 5). Because protein aggregates were detected in sensory processes in the head, we tested for effects on chemosensation (45) in animals expressing full-length and truncated ATXN3. AT3q130 animals showed a slight reduction in chemotaxis index (Ci) to isoamyl alcohol (10^{-1} dilution) relative to WT animals (Supplementary Material, Fig. S7), and 257cAT3q75, but not Q40 animals showed a significant decrease in Ci (Supplementary Material, Fig. S7; $^*P < 0.05$).

Taken together, these results suggest that the presence of aggregates is associated with neuronal dysfunction in our *C. elegans* model of ATXN3 pathogenesis. Moreover, the

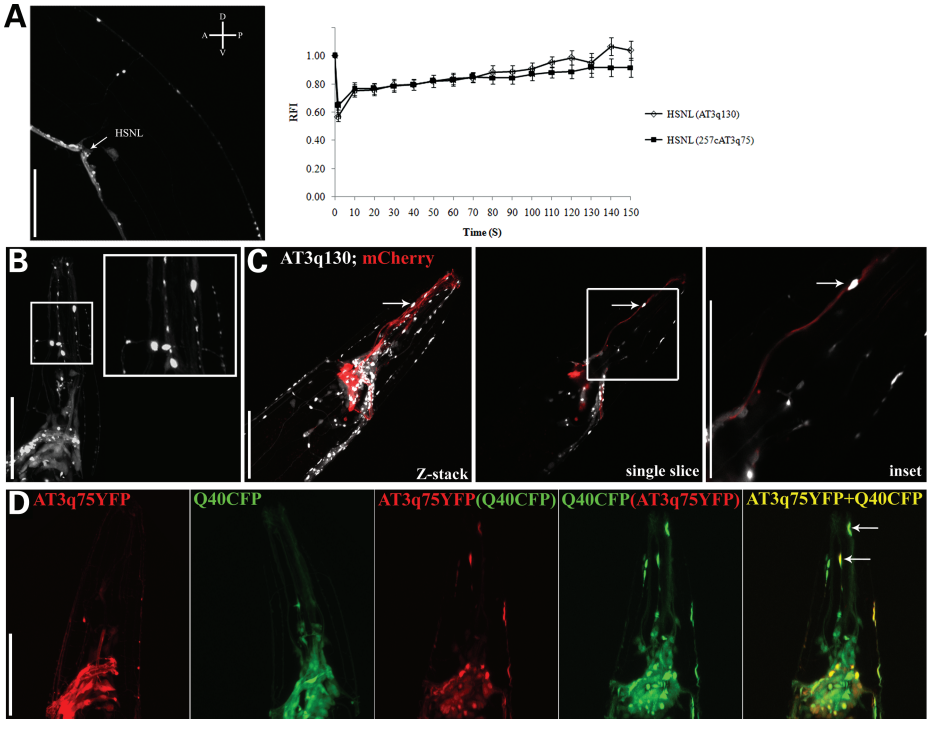

Figure 4. The aggregation pattern of mutant ATXN3 in specific neuronal cells is not stochastic. FRAP analysis of the HSN neuron on the left side (**A**) of AT3q130 and 257cAT3q75 animals revealed that both proteins were consistently soluble (at least 80% FRAP) in the two or three independent lines that were tested for each genotype. Quantification was performed in 10 or more experiments and is represented as the mean ± SEM. (A) Flattened z-series of *C. elegans* heads expressing mutant ataxin-3 proteins showed the presence of aggregates in certain neuronal processes [a 257cAT3q75 day 4 animal is shown as an example in (**B**)]. White box indicates the magnified region. The aggregates co-localized with mCherry proteins that were expressed under the regulation of the CHE-13 promoter (**C**). (C) depicts a z-stack (first panel) and a single slice (second panel), showing one aggregate co-localizing with the sensory neuron process (red) (C, arrows). Flattened z-stacks of day 4 animals co-expressing AT3q75::YFP with Q40::CFP proteins, showing protein aggregates in certain sensory processes of the head (**D**, arrows). The first panel shows the head of one animal expressing AT3q75 proteins; the second panel shows one animal expressing Q40 proteins; third and fourth panels show the expression of AT3q75 or Q40 proteins of a AT3q75; Q40 animal; fifth panel displays a merged image. (**E**) Quantification of the aggregates of the sensory processes of AT3q75;Q40 in comparison with AT3q14;Q40 animals (Supplementary Material, Fig. S6A). In all images, scale bar = 50 μm. The images were obtained using either an Olympus (A and C) or a Zeiss LSM 510 (B and D) confocal microscope. FRAP measurements (A) were performed using the Olympus FV100 confocal.

expression of full-length AT3q130, C-terminal 257cAT3q80 and Q40 proteins caused the same level of toxicity (Fig. 5, dashed line) highlighting the modulatory effects of flanking protein regions in polyQ-containing proteins on motor dysfunction.

Age-dependent changes in mutant ataxin-3 aggregation dynamics

The risk of developing a neurodegenerative disease increases with age. Previous work has shown that polyQ aggregation progresses in an age-dependent manner in muscle cells (36) and in specific neurons (23,33). Therefore, we analyzed the aggregation profile of ATXN3 transgenic animals during aging. In AT3q130 animals, aggregation (initially detected at day 1 post-hatching; Supplementary Material, Fig. S4) was observed to increase during aging. This was particularly clear in the anterior and ventral ganglia neurons in the nerve ring (Fig. 6A). Heterogeneity in protein solubility and aggregation persisted in the nerve cords during aging (data not shown). Of the C-terminal fragments, 257cAT3q75- and 257cAT3q80-expressing animals showed age-dependent aggregation (Fig. 6B). For both the full-length and C-terminal ATXN3 proteins, aggregates were not detected in HSN neurons of old animals. In comparison, AT3q75 did not form aggregates during aging; however in some animals, we observed large foci in day 10 of adulthood that corresponded to a soluble protein (Fig. 6A, arrows) by FRAP analysis (data not shown). Likewise, animals expressing WT (full-length and truncated) ATXN3 did not form aggregates during their lifespan. These results reveal that aging contributes to the onset and progression of ATXN3 polyQ aggregation, as has been reported for other model systems and humans. However, our ability to monitor the aggregation phenotypes across multiple subclasses of neurons reveals differential susceptibility, with certain neurons such as the HSN more resistant to aggregation compared with the VNC and DNC neurons that are more sensitive to aggregation during aging.

IIS and HSF-1 pathways modify mutant ataxin-3-mediated pathogenesis in *C. elegans*

Aggregation and toxicity of polyQ are strongly affected by the IIS pathway and the activities of transcription factors DAF-16 and HSF-1 (21,36). To test whether ataxin-3 proteotoxicity is influenced by these pathways, we examined the effects of

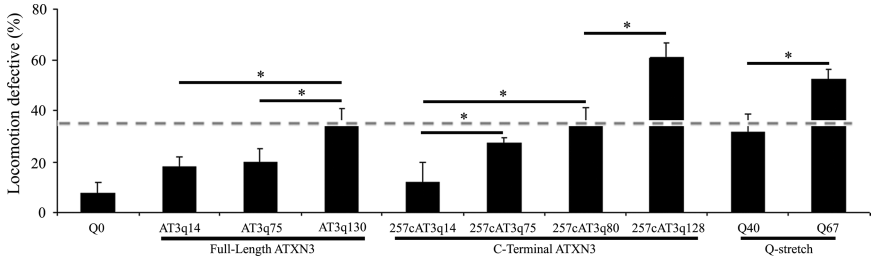

Figure 5. Increases in polyQ-length associated with neuronal dysfunction in ataxin-3 *C. elegans* model. Percentage of locomotion defective of age-synchronized young adult animals (day 4, post-hatching). There was a polyQ length-dependent increase in motor dysfunction in both full-length and C-terminal ATXN3-expressing animals. Q(n) lines were used as an experimental control. ATXN3 protein-flanking sequences modulate the animals' motor phenotype. Dashed line shows that the expression of AT3q130, 257cAT3q80 and Q40 proteins in all neurons caused similar percentages of defect in locomotion. Data are the mean ± SD, at least 150 animals per data point. Student's *t*-test, $^{*}P < 0.05$.

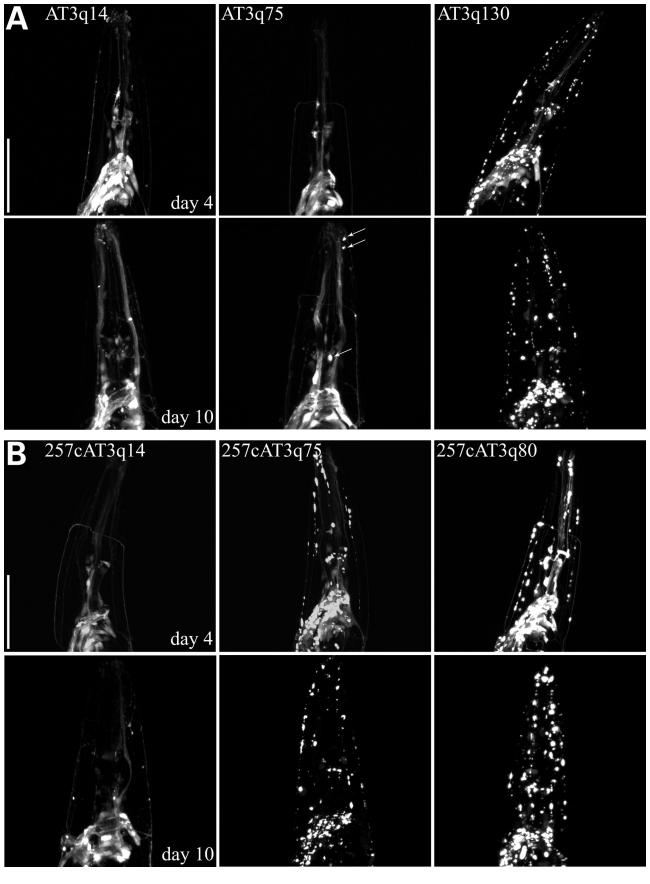

Figure 6. Influence of age on mutant ATXN3 aggregation dynamics. Flattened z-stacks of *C. elegans* heads of days 4 and 10 animals (post-hatching). The aggregation phenotype of AT3q130 (**A**) and 257cAT3q75/80 (**B**) animals was aggravated with age. The increase in aggregation was particularly evident in the circumpharyngeal nerve ring of the animals. Arrows in the AT3q75 panel indicate protein foci that did not correspond to aggregates, as assessed by FRAP (data not shown). Scale bar, 50 μm. All pictures were obtained using a Zeiss LSM 510 confocal microscope.

mutations in the insulin/IGF-1 receptor DAF-2 (46) on the properties of AT3q130. In the background of the *daf-2(e1370)* mutation, which confers a long-lived phenotype, animals expressing AT3q130 (*daf-2*; AT3q130) showed a tendency for decreased aggregation (Fig. 7A, squares, and F) with foci barely detected. Likewise, motor function improved 2-fold (from 46.8 to 25.6%) in *daf-2*; AT3q130 animals (Fig. 7G). Similar results were obtained with a loss-of-function allele (*hx546*) in *age-1* (47) that restored the motility of AT3q130 animals from 40% reduction to 14.7% (Fig. 7G). These results support the role of DAF-16 (48,49) in protection against proteotoxicity. Consistent with this, the *daf-16* null (*mu86*) allele had a major effect on motor dysfunction in *C. elegans daf-16*; AT3q130 animals (from 40.1 to 74.4%) (Fig. 7H). We further demonstrated a protective role for DAF-16 with valproic acid (VA) that stimulates the translocation of DAF-16 into the nucleus (50). VA partially rescued the motor dysfunction induced by AT3q130 expression, at day 10 of adulthood (a reduction in motility impairment from 71.8 to 37.9%), an effect that was suppressed in *daf-16(mu86)* mutants, suggesting that the mode of action for the rescue of mutant-ATXN3 toxicity was in part through the IIS pathway (Fig. 8A). Moreover, day 10 AT3q130 VA-treated animals showed the same locomotion defect as day 4 untreated animals. In contrast to the significant phenotype effect, and as for *daf-16(mu86)* mutation (Fig. 7D and F), VA treatment had only a mild effect on AT3q130 protein aggregation (Fig. 8B), which was not due to changes in AT3q130 protein levels (Supplementary Material, Fig. S8). In all cases, the effects of mutations in *DAF-2*, *AGE-1* and *DAF-16* genes in ATXN3 pathogenesis were not due to effects on AT3q130 expression (Supplementary Material, Fig. S9).

Recent studies have also implicated HSF-1 in lifespan extension caused by reduced DAF-2 activity, with cross-talk between the DAF-2 and HSF-1 pathways (20,21). Therefore, we tested the effect of the *hsf-1(sy441)* (51) mutation on ATXN3 pathogenesis. The loss of *hsf-1* was deleterious to transgenic animals, with mutant ataxin-3 proteins becoming fully aggregated in neuronal cells and detected in early embryos (Fig. 7E, arrow). Moreover, *hsf-1*; AT3q130 animals were completely paralyzed at day 4 (Fig. 7H). Consistent with these results, exposure of AT3q130 animals to the small-molecule Hsp90 inhibitor, 17-(dimethylaminoethylamino)-17-demethoxygeldanamycin (17-DMAG), that induces the heat shock response (HSR), improved motility when compared with untreated controls (Fig. 8C). The effect of 17-DMAG was dependent on *hsf-1* (Fig. 8C). Treatment with 17-DMAG also reduced the aggregation of AT3q130 animals (Fig. 8D), with no effect on ATXN3 steady-state

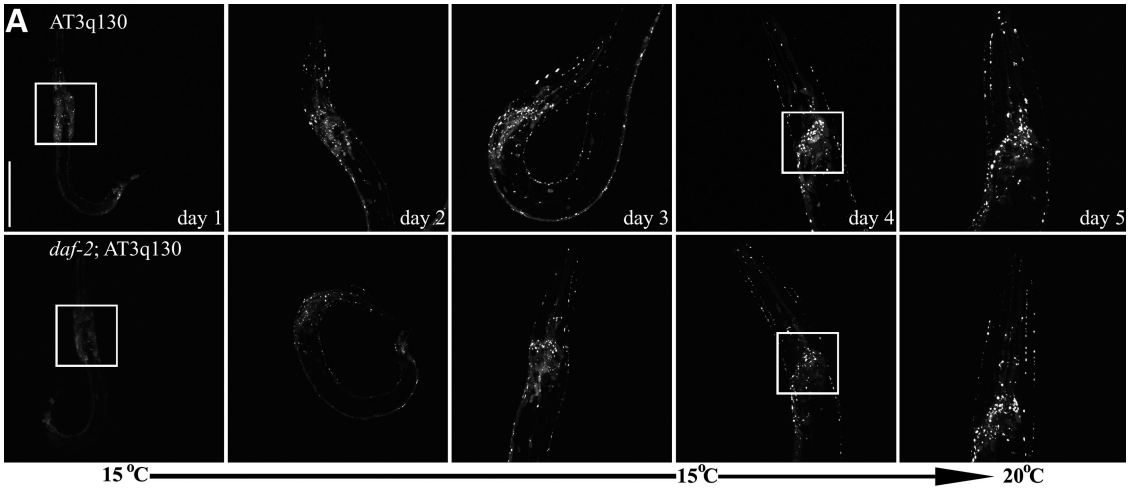

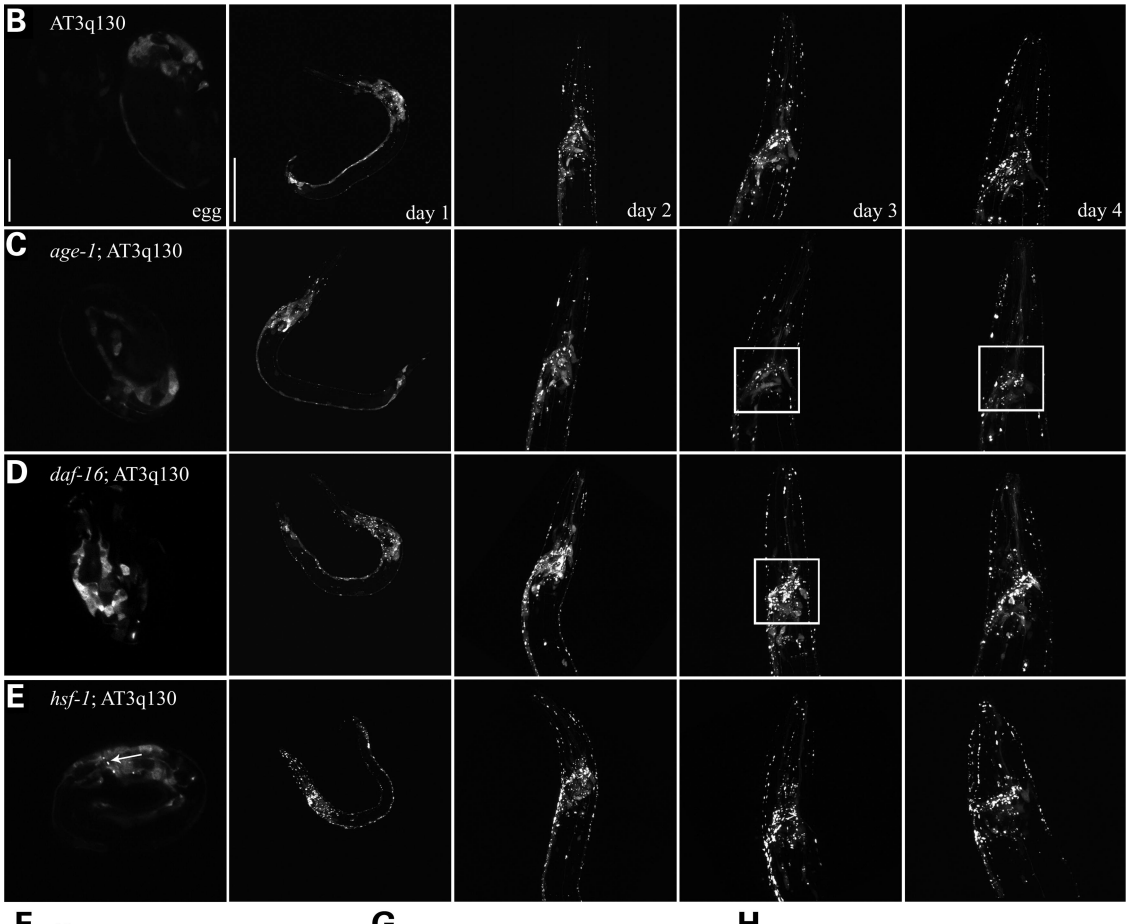

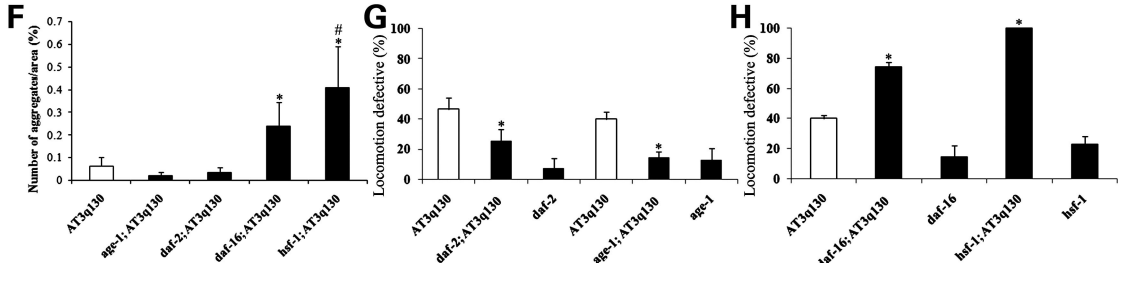

protein levels (Supplementary Material, Fig. S8). 17-DMAG treatment still decreased the locomotion impairment of AT3q130 animals in the absence of DAF-16 (Supplemental Material, Fig. S10).

Interestingly, at early disease stages, mutation in *hsf-1* caused a more severe effect on AT3q130 aggregation, when compared with *daf-16*. Quantification of the aggregates (42) at day 1 revealed that the absence of HSF-1 significantly increased the percentage number of aggregates per total area when compared with *daf-16*; AT3q130 and AT3q130 animals ($^{\#}P < 0.05$, Fig. 7F). Moreover, quantification of the aggregates in specific areas of the nervous system revealed that total body aggregation correlates with aggregation in the animals head (nerve ring and head processes) and in the VNC (Supplemental Material, Fig. S11). Both total body aggregation (Fig. 7F) and neuron-specific aggregation (Supplemental Material, Fig. S12) are modified by IIS and HSF-1.

Taken together, these results demonstrate that ATXN3 proteotoxicity is strongly modulated by aging-related cellular changes, associated with the IIS pathway and the HSR.

DISCUSSION

We describe a new model system for human ATXN3 proteotoxicity in *C. elegans* neuronal cells, in which the use of tissue-specific promoters and the ability to monitor the fluorescence of reporter proteins in different neurons of live animals (by microscopy and dynamic imaging analysis) provides an effective means to continuously evaluate mutant ATXN3 aggregation and pathogenesis. We have taken advantage of the single-cell resolution of the FRAP analysis to scrutinize the solubility of ATXN3 in specific neuronal subtypes. In *C. elegans*, ATXN3-flanking sequences greatly modulate polyQ-mediated aggregation and neuronal dysfunction. The neuronal cell-type-specific susceptibility to expression of mutant ATXN3 proteins is not stochastic and differs significantly from that of polyQ-alone. We also show that mutant ATXN3 phenotypes are severely aggravated during aging and demonstrate the protective roles of the DAF-16 and HSF-1 pathways to suppress proteotoxicity.

Caenorhabditis elegans model for ATXN3 aggregation and neuronal dysfunction

In our *C. elegans* model, we observed the polyQ length-dependent aggregation of both full-length and C-terminal versions of mutant ATXN3 proteins expressed in *C. elegans*. Although ataxin-3 cleavage-fragment formation has not been unequivocally shown *in vivo*, many laboratories have proposed that smaller fragments containing the expanded polyQ sequence exhibit enhanced toxicity (25,38,40,41,52). Likewise, we show the importance of sequence context in that expression of 75 Qs leads to the formation of protein aggregates in the *C. elegans* nervous system within C-terminal ATXN3 flanking regions, but not in the full-length protein. This is likely due to the increased exposure of the polyQ tract in the truncated version of the protein, which eventually facilitates (i) misfolding and (ii) abnormal toxic interactions in the cellular environment of the affected neurons. There are several lines of evidence that support this hypothesis, namely that Q40 has been described as the Q-length threshold for aggregation and toxicity (32). Moreover, the majority of studies using cell lines, *Drosophila* and mouse models of MJD showed stronger phenotypes with truncated polyQ-containing versions of ATXN3 (24,41,53); in some cases, the full-length mutant ATXN3 did not cause pathogenesis (41,53). Regarding potential abnormal toxic interactions in the affected cellular environment, it has been reported that the presence of an expanded polyQ tract facilitates and strengthens the interaction between the C-terminal of ATXN3 and VCP (54), CBP and the transcriptional co-activators p300 and pCAF (55). These abnormal interactions may affect basic cellular maintenance mechanisms such as endoplasmic reticulum-associated protein degradation (56) and transcriptional regulation (55,57).

ATXN3-flanking sequences and cell-intrinsic factors may direct neuronal cell-type-specific susceptibility

Each of the polyQ disorders involves the loss of selected populations of neurons, leading to a characteristic clinical presentation, even though the mutant proteins are ubiquitously expressed (6). As in the human disease, we found that the neuronal cell-type susceptibility to mutant ATXN3 protein aggregation and toxicity in the *C. elegans* nervous system was not stochastic, but was rather neuron-type-specific and observed in multiple animals and transgenic lines.

A key finding here is that the aggregation pattern of ATXN3- and polyQ-expressing animals is quite distinct. Mutant ataxin-3 aggregates in several neuronal processes, including commissures, the DNC and sensory processes. In particular, the processes of certain CHE-13-positive sensory neurons contain protein foci only when the polyQ tract is expressed within ATXN3-flanking sequences and not when expressed alone (32). Although the cell bodies of lateral neurons contained soluble ataxin-3 proteins, even in very old animals, their processes often presented aggregates as

Figure 7. IIS and HSF-1 pathways regulated mutant ataxin-3-mediated proteotoxicity in *C. elegans* neurons. (**A**) Flattened z-series of AT3q130 and *daf-2*; AT3q130 animals that were grown at 15°C for 4 days and transferred to 20°C for 24 h. (**B**–**E**) Animals were grown at 20°C during their lifespan. White squares highlight the area where the decrease in aggregation is most clear. (A, B and **F**) *daf-2(e1370)* and *age-1(hx546)* mutations tend to reduce AT3q130-mediated aggregation. The absence of DAF-16 (D) and HSF-1 (E) increased aggregation of mutant ATXN3 (F). The *daf-16(mu86)* mutation caused a mild aggravation of the aggregation phenotype, visible at day 3 (post-hatching) (D, square). *hsf-1(sy441)* (E) mutation had a great impact on aggregation, with some aggregates visible already in embryos (arrow). Scale bar, 50 μm. All pictures were obtained using an Olympus FV1000 confocal microscope. (F) Quantification of the number of aggregates per area of animal of all strains. Data show the mean ± SD of eight or more animals. Asterisk indicates the significant mean difference between either *hsf-1*; AT3q130 or *daf-16*; AT3q130 and AT3q130 animals; hash symbol indicates the significant difference between *hsf-1*; AT3q130 and *daf-16*; AT3q130 (*ANOVA*, applying *Bonferroni* correction with 95% confidence intervals; $^{*,\#}P < 0.05$). (**G** and **H**) *daf-2* and *age-1* mutations reduced the percentage of motor dysfunction (from 46.8 to 25.6% and 40 to 14.7% reduction, respectively). *daf-16* and *hsf-1* mutations caused an increase in the % of locomotion defective animals (from 40.1 to 74.4% and 40.1 to 100%, respectively). Data are the mean ± SD, at least 102 animals per data point. Student's *t*-test, $^{*}P < 0.05$.

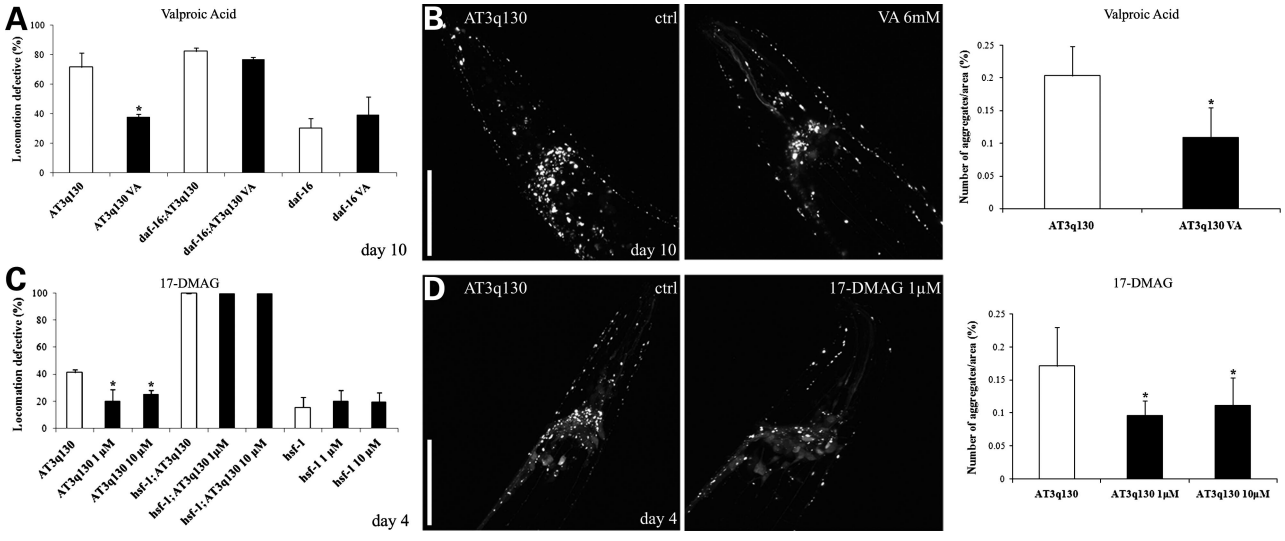

Figure 8. Pharmacological activation of DAF-16 and HSF-1 reduced mutant ataxin-3-mediated pathogenesis. VA-treated AT3q130 animals showed a reduction both in motor dysfunction (71.75% to 37.9% reduction in locomotion defective animals) (**A**) and in the aggregation phenotype at day 10 of adulthood (**B**). Despite the broad actions of VA, the effect on ATXN3 pathogenesis seemed to be highly dependent on DAF-16 (A). Day 4 animals treated with two concentrations of 17-DMAG also improved their motility performance. The effect of 17-DMAG on motor function was dependent on *hsf-1* (**C**). Animals also showed a reduction in aggregation (**D**). Motility data are the mean ± SD, at least 152 animals per data point. Student's *t*-test, $^{*}P < 0.05$. Quantification of number of aggregates per area is the mean ± SD of eight or more animals per group. ANOVA, $^{*}P < 0.05$.

determined by FRAP. By comparison, these processes were unaffected in Q40 animals (32). In agreement with these observations, a recent systematic immunohistochemical analysis of serial thick brain sections of MJD patients revealed the widespread presence of axonal aggregates in fiber tracts known to undergo neurodegeneration (58). This may be related to the protein cellular function since the josephin domain of ATXN3 was found to bind to alpha- and beta-tubulin in human cells and rat brain extracts (59,60) and that ATXN3 knock-down led to cytoskeletal disorganization (59). These results imply that ATXN3-flanking sequences, other than the polyQ stretch, in conjunction with cell-specific factors, may modulate neuronal vulnerability.

Recent studies have suggested that the specific symptoms of a given misfolding disorder, namely amyotrophic lateral sclerosis, may not be due solely to aggregation-mediated toxicity of SOD1 mutations, but also to their genetic interactions with mildly destabilizing missense temperature-sensitive alleles within a variety of cellular pathways (61). Studies in HD have also identified the small G protein Rhes, which is expressed and localized very selectively to the striatum, as an interactor of mutant huntingtin, contributing to cytotoxicity (62). These studies, together with our results, emphasize the importance of understanding the role of protein context in diseases characterized by protein aggregation.

Intriguingly, in both full-length and truncated ATXN3 models, the same neurons were affected, although at different ages or polyQ lengths. The fact that we have observed similar neuropathology in animals expressing the ATXN3 cleavage fragment lends support to the relevance of ataxin-3 fragment formation in MJD pathogenesis. However, additional experiments are required to determine the protein domain(s) of ATXN3 that determine the neuronal specificity of polyQ-mediated pathogenesis.

IIS- and HSF-1-mediated improved proteostasis protect against mutant ataxin-3 pathogenesis

Aging is a prominent determinant of the structural and functional changes that may contribute to the decline in brain function and susceptibility to neurodegenerative disease (63). The age-related IIS and HSF-1 pathway(s) are known to modulate many forms of toxic protein aggregation in *C. elegans* and other model organisms, including the aggregation of Aβ (22,64), α-synuclein (65,66), polyQ and huntingtin (20,36,67), suggesting that these pathways correspond to a common mechanism of detoxification. However, for MJD, the roles of the IIS and HSF-1 pathways had not been previously examined. In this study, we have shown that aging intensifies mutant ATXN3 aggregation and motor dysfunction. Moreover, neuronal toxicity was significantly affected by altering the aging/survival program. Specifically, DAF-16 and HSF-1 were found to be potent suppressors of mutant ataxin-3 aggregation and neuronal dysfunction in *C. elegans*. The absence of HSF-1 accelerated aggregation at early stages of development (embryos), whereas in a *daf-16* mutant, increased aggregation was more pronounced in adult animals. In agreement, VA-treated animals showed reduced aggregation and motor dysfunction later in life (day 10), which was dependent upon DAF-16. Aggregate quantification in day 1 animals further supported this finding, as we also showed that mutant ATXN3 aggregation was greatly enhanced by the *hsf-1* mutation compared with *daf-16*. This supports the proposal that HSF-1 and DAF-16 have different developmental requirements—early embryonic for HSF-1 versus adult for DAF-16—in protection against proteotoxicity as observed previously in a *C. elegans* model for Alzheimer's disease (68). In future studies, we aim to test whether the effects of DAF-16 and HSF-1 loss of function in mutant ATXN3-mediated pathogenesis are due to neuronal effects.

Transcriptomes regulated by DAF-16 and HSF-1 include mRNAs for many chaperones (20,21). In this sense, our results are in agreement with studies showing that, in the brain tissue of MJD patients, Hsp40 and Hsp70 localize to intranuclear aggregates (possibly causing a depletion of these chaperones) and that overexpression of the human DnaJ homolog (Hdj)-1 suppressed ATXN3 aggregation and toxicity in neuronal cell cultures (69). Moreover, knocking out the co-chaperone C-terminus of Hsp70-interacting protein enhanced ataxin-3 aggregation-mediated toxicity (70). Consistent with our results using a genetic approach, pharmacological treatment with 17-DMAG reduced mutant-ATXN3 proteotoxicity in *C. elegans*, probably by activating the disaggregation capacity of HSF-1 at early stages of the disease (22,68).

In conclusion, our study supports a link between lifespan determinants, integrity of protein folding and amelioration of aggregation-associated proteotoxicity in MJD. Our novel *C. elegans* ATXN3 pathogenesis model may constitute a useful tool for high-throughput testing of therapeutic strategies in age-related conformational disorders. Additionally, comparison of our system with the previously established polyQ protein-alone models and with *C. elegans* models for the pathogenesis of the different disease-associated proteins (huntingtin, androgen receptor or ataxin-1) could allow the clarification of both common and protein-specific mechanism(s) of aggregation, neuronal dysfunction and neurodegeneration.

MATERIALS AND METHODS

Plasmid constructs

Pan-neuronal ATXN3 expression was achieved by cloning AT3var1−1 cDNA into the $P_{F25B3.3}$Q0::YFP plasmid (32). F25B3.3::GFP is a post-mitotic pan-neuronal marker; its expression is observed after the terminal division of neurons and not in neuroblasts (37). Full-length ATXN3 cDNA with different polyQ lengths was generated by PCR using oligonucleotides containing restriction sites for *Bam*HI and pBluescriptIISK(+)::MJD1−1q14 or pGEM-7Zf(+)::MJD1−1q75 (kindly provided by Dr Jun Goto) as templates. ATXN3 amplicons were then digested and ligated into the *Bam*HI sites of $P_{F25B3.3}$Q0::YFP, generating $P_{F25B3.3}$AT3v1−1q(n)::YFP. Regarding the cloning of $P_{F25B3.3}$AT3v1−1q(130)::YFP, the first step was to subclone the tract of 130Qs from pPD95.77::Punc119::MJD1−130Q (kindly provided by Dr N. Nukina) into the *Bgl*II and *Eco*0109I restriction sites of pGEM-7Zf(+)::MJD1−1q75 vector. ATXN3 C-terminal YFP-tagged expression constructs were generated by PCR (using full-length constructs as a template) and cloned into the *Bam*HI sites of $P_{F25B3.3}$Q0::YFP, forming $P_{F25B3.3}$257cAT3q(n)::YFP. Sequencing confirmed the ATXN3 sequence (full-length and truncated forms), including the Q-length and YFP sequences, as well as the promoter region.

Nematode strains and general methods

For a list of strains used in this work and name abbreviations, see Supplementary Material, Table S1. Standard methods were used for culturing and observing *C. elegans*, unless otherwise noted (71). Nematodes were grown on NGM plates seeded with *Escherichia coli* OP50 strain at 20°C. All strains carrying the *daf-2* mutation (*e1370* allele) were grown at 15°C until the L4 stage and were then transferred to 20°C for 24 h. For the generation of transgenic neuronal animals, 50 ng/μl of DNA encoding $P_{F25B3.3}$AT3q(n)::YFP and $P_{F25B3.3}$257-cAT3q(n)::YFP was microinjected into the gonads of adult hermaphrodite N2 animals, as previously reported (32). Transgenic F1 progeny were selected on the basis of neuronal fluorescence. At least three independent stable lines for each transgene were isolated and analyzed, with similar results. Transgenic lines were frozen immediately after they were generated, as it has been previously reported that animals kept in continuous culture, particularly those expressing expanded polyQ tracts, eventually adapt to the transgene (72). Integrated lines were generated by gamma irradiation of transgenic animals expressing AT3q(n)::YFP and 257cAT3q(n)::YFP fusion proteins, allowing uniform expression of transgenes. Two or three independent lines were isolated and backcrossed at least five times with N2. P_{CHE-13}::mCherry DNA (PS431, kindly provided by Peter Swoboda, Karolinska Institute) was microinjected into adult hermaphrodite AT3q130 animals at 10 ng/μl. Populations were synchronized either by treating young adult animals with alkaline hypochlorite solution (0.5 M NaOH, ∼2.6% NaClO) for 7 min (73) or by collecting embryos laid by adult animals within a 3 h period. All animals were scored at the same chronological age, unless stated otherwise. During the reproductive period, animals were moved every day to avoid progeny contamination. Experiments were repeated at least three times. All assays were performed blind.

Confocal imaging

All images were captured either on a Zeiss LSM510 META (Oberkochen, Germany) or on an Olympus FV1000 (Japan) confocal microscope, under a 63× water or 60× oil objective, respectively. Animals were immobilized with 2 mM levamisole and mounted on a 3% agarose pad. Z-series imaging was taken of all the *C. elegans* lines generated, using 514/515 nm laser excitation for YFP, 458 nm for CFP and 593 nm for mCherry fusion proteins. The pinhole was adjusted to 1.0 Airy unit of optical slice, and a scan was taken every ∼0.5 μm along the *Z*-axis. Immobilized 4- or 10-day-old animals were subjected to FRAP as previously described (74) with the following modifications: imaging of full-length, C-terminal ATXN3 and ATXN3;Q40 animals was performed at 5% power of a 514 nm laser line with the bleaching power of 100% for 25 iterations. Relative fluorescence intensity (RFI) was determined using the following equation: RFI = (Tt/Ct)/(T0/C0), in which T0 is the total intensity of the region of interest (ROI) prior to photobleaching and Tt is the intensity of the same area at a given time after bleaching. The intensities were normalized against a non-bleached ROI within the same cell (C0, intensity of the control area prior to bleaching and Ct at any time after) as a control for general photobleaching and background fluorescence (74). FRAP analysis was consistently performed in all animals in at least six VNC (adjoining the vulva), DNC (opposing the

vulva) cells, head neurons and tail neurons (cell bodies and/or processes). FRAP of HSN neurons was performed on an Olympus FV1000 confocal microscope (1% power of a 515 nm laser line with bleaching power of 50%, using the Tornado scanning mode).

Quantification of the aggregates

Caenorhabditis elegans fluorescent images were acquired using the Olympus FV1000 confocal microscope. Confocal microscope parameters were set using Hi-Lo pallet, such that protein foci and not diffuse fluorescent areas of the animals nervous system presented pixel intensity higher than 255. The z-stack was collapsed and the aggregate load of each animal (per area unit) was calculated on an image-processing application using MeVisLab as a platform. Details on the application and on the segmentation algorithms were described elsewhere (42). At least eight images were analyzed per genotype and statistical assessment was performed using the Origin software (OriginLab) (ANOVA and Bonferroni mean correction tests for multiple comparisons).

Motility assay

All assays were performed at room temperature (~20°C) using synchronized animals grown at 15°C or 20°C. Five animals (4-, 5- or 10-day-old) were placed simultaneously in the middle of a freshly seeded plate, equilibrated at 20°C. Animals remaining inside a 1 cm circle after 1 min were scored as locomotion-defective. A total of 150 animals were scored in at least three independent assays for each strain, and the statistical significance was assessed by Student's *t*-test, as described previously (44).

VA treatment

VA treatment was performed according to the protocol described by Evason *et al.* (50). VA sodium salt was obtained from Sigma (St Louis, MO, USA). Animals were always grown in 6 mM VA plates at least one generation prior to the beginning of the assay and were kept in the dark. After 10 days (post-hatching), animals were scored for motility defects and alteration in the aggregation profile, using confocal imaging.

17-DMAG treatment

Drug assays were performed in 96-well plates in liquid culture, as previously described (43,75). Each well contained a final volume of 60 µl, including 20–25 animals in egg stage, drug at the appropriate concentration and OP50 bacteria to a final OD of 0.8 in the microtiter plate (Bio-Rad). Animals and bacteria were resuspended in S-medium supplemented with streptomycin, penicillin and nystatin (Sigma). Worms were grown with continuous shaking at 180 rpm at 20°C. Compound preparation: a stock solution of 16.2 mM 17-DMAG (NCS707545, InvivoGen) was prepared in water. On the indicated days, animals were imaged using a confocal microscope (Olympus FV1000) and tested for motility defects.

SUPPLEMENTARY MATERIAL

Supplementary Material is available at *HMG* online.

ACKNOWLEDGEMENTS

We are grateful to members of the Maciel and Morimoto laboratories for sharing reagents, for critical analysis of the data and for their helpful discussions on the manuscript. We thank Jun Goto (The University of Tokyo Hospital), David Pilgrim (University of Alberta), Nobuyuki Nukina (RIKEN Brain Science Institute) and Peter Swoboda (Karolinska Institute) for generously sharing reagents; we thank Thomas O'Halloran and Biological Imaging Facility (Northwestern University) for the use of microscopes. A special thanks to the *Caenorhabditis* Genetics Center (CGC), which is funded by the National Institutes of Health – National Center for Research Resources, for some of the nematode strains.

Conflict of Interest statement. None declared.

FUNDING

This work was supported by grants from Fundação Ciência e Tecnologia (FCT) to P.M. (PTDC/SAU-GMG/64076/2006, PTDC/SAU-GMG/112617/2009, SFRH/BD/27258/2006 to A.T.C., UMINHO/BI/052/2010 to A.J. and SFRH/BD/51059/2010 to A.N.C.), from the National Ataxia Foundation to PM and from the National Institutes of Health (NIGMS, NIA and NINDS) to R.M. This work was also granted by the Hospital San Rafael (Coruña) with the Rafael Hervada prize on Biomedical Research (2010).

REFERENCES

1. Schols, L., Amoiridis, G., Langkafel, M., Buttner, T., Przuntek, H., Riess, O., Vieira-Saecker, A.M. and Epplen, J.T. (1995) Machado–Joseph disease mutations as the genetic basis of most spinocerebellar ataxias in Germany. *J. Neurol. Neurosurg. Psychiatry*, **59**, 449–450.
2. Schols, L., Bauer, P., Schmidt, T., Schulte, T. and Riess, O. (2004) Autosomal dominant cerebellar ataxias: clinical features, genetics, and pathogenesis. *Lancet Neurol.*, **3**, 291–304.
3. Coutinho, P. and Andrade, C. (1978) Autosomal dominant system degeneration in Portuguese families of the Azores Islands. A new genetic disorder involving cerebellar, pyramidal, extrapyramidal and spinal cord motor functions. *Neurology*, **28**, 703–709.
4. Gatchel, J.R. and Zoghbi, H.Y. (2005) Diseases of unstable repeat expansion: mechanisms and common principles. *Nat. Rev. Genet.*, **6**, 743–755.
5. Perutz, M.F. (1999) Glutamine repeats and neurodegenerative diseases: molecular aspects. *Trends Biochem. Sci.*, **24**, 58–63.
6. Ross, C.A. (1995) When more is less: pathogenesis of glutamine repeat neurodegenerative diseases. *Neuron*, **15**, 493–496.
7. do Carmo Costa, M., Gomes-da-Silva, J., Miranda, C.J., Sequeiros, J., Santos, M.M. and Maciel, P. (2004) Genomic structure, promoter activity, and developmental expression of the mouse homologue of the Machado–Joseph disease (MJD) gene. *Genomics*, **84**, 361–373.
8. Rodrigues, A.J., Coppola, G., Santos, C., Costa Mdo, C., Ailion, M., Sequeiros, J., Geschwind, D.H. and Maciel, P. (2007) Functional genomics and biochemical characterization of the *C. elegans* orthologue of the Machado–Joseph disease protein ataxin-3. *FASEB J.*, **21**, 1126–1136.
9. Doss-Pepe, E.W., Stenroos, E.S., Johnson, W.G. and Madura, K. (2003) Ataxin-3 interactions with rad23 and valosin-containing protein and its

associations with ubiquitin chains and the proteasome are consistent with a role in ubiquitin-mediated proteolysis. *Mol. Cell. Biol.*, **23**, 6469–6483.
10. Burnett, B., Li, F. and Pittman, R.N. (2003) The polyglutamine neurodegenerative protein ataxin-3 binds polyubiquitylated proteins and has ubiquitin protease activity. *Hum. Mol. Genet.*, **12**, 3195–3205.
11. Donaldson, K.M., Li, W., Ching, K.A., Batalov, S., Tsai, C.C. and Joazeiro, C.A. (2003) Ubiquitin-mediated sequestration of normal cellular proteins into polyglutamine aggregates. *Proc. Natl Acad. Sci. USA*, **100**, 8892–8897.
12. Chow, M.K., Mackay, J.P., Whisstock, J.C., Scanlon, M.J. and Bottomley, S.P. (2004) Structural and functional analysis of the Josephin domain of the polyglutamine protein ataxin-3. *Biochem. Biophys. Res. Commun.*, **322**, 387–394.
13. Ferro, A., Carvalho, A.L., Teixeira-Castro, A., Almeida, C., Tome, R.J., Cortes, L., Rodrigues, A.J., Logarinho, E., Sequeiros, J., Macedo-Ribeiro, S. *et al.* (2007) NEDD8: a new ataxin-3 interactor. *Biochim. Biophys. Acta.*, **1773**, 1619–1627.
14. Sequeiros, J. and Coutinho, P. (1993) Epidemiology and clinical aspects of Machado–Joseph disease. *Adv. Neurol.*, **61**, 139–153.
15. Riess, O., Rub, U., Pastore, A., Bauer, P. and Schols, L. (2008) SCA3: neurological features, pathogenesis and animal models. *Cerebellum*, **7**, 125–137.
16. Lin, M.T. and Beal, M.F. (2006) Mitochondrial dysfunction and oxidative stress in neurodegenerative diseases. *Nature*, **443**, 787–795.
17. Amaducci, L. and Tesco, G. (1994) Aging as a major risk for degenerative diseases of the central nervous system. *Curr. Opin. Neurol.*, **7**, 283–286.
18. Cohen, E. and Dillin, A. (2008) The insulin paradox: aging, proteotoxicity and neurodegeneration. *Nat. Rev. Neurosci.*, **9**, 759–767.
19. Ben-Zvi, A., Miller, E.A. and Morimoto, R.I. (2009) Collapse of proteostasis represents an early molecular event in *Caenorhabditis elegans* aging. *Proc. Natl Acad. Sci. USA*, **106**, 14914–14919.
20. Hsu, A.L., Murphy, C.T. and Kenyon, C. (2003) Regulation of aging and age-related disease by DAF-16 and heat-shock factor. *Science*, **300**, 1142–1145.
21. Morley, J.F. and Morimoto, R.I. (2004) Regulation of longevity in *Caenorhabditis elegans* by heat shock factor and molecular chaperones. *Mol. Biol. Cell*, **15**, 657–664.
22. Cohen, E., Bieschke, J., Perciavalle, R.M., Kelly, J.W. and Dillin, A. (2006) Opposing activities protect against age-onset proteotoxicity. *Science*, **313**, 1604–1610.
23. Khan, L.A., Bauer, P.O., Miyazaki, H., Lindenberg, K.S., Landwehrmeyer, B.G. and Nukina, N. (2006) Expanded polyglutamines impair synaptic transmission and ubiquitin–proteasome system in *Caenorhabditis elegans*. *J. Neurochem.*, **98**, 576–587.
24. Warrick, J.M., Morabito, L.M., Bilen, J., Gordesky-Gold, B., Faust, L.Z., Paulson, H.L. and Bonini, N.M. (2005) Ataxin-3 suppresses polyglutamine neurodegeneration in *Drosophila* by a ubiquitin-associated mechanism. *Mol. Cell*, **18**, 37–48.
25. Goti, D., Katzen, S.M., Mez, J., Kurtis, N., Kiluk, J., Ben-Haiem, L., Jenkins, N.A., Copeland, N.G., Kakizuka, A., Sharp, A.H. *et al.* (2004) A mutant ataxin-3 putative-cleavage fragment in brains of Machado–Joseph disease patients and transgenic mice is cytotoxic above a critical concentration. *J. Neurosci.*, **24**, 10266–10279.
26. Bichelmeier, U., Schmidt, T., Hubener, J., Boy, J., Ruttiger, L., Habig, K., Poths, S., Bonin, M., Knipper, M., Schmidt, W.J. *et al.* (2007) Nuclear localization of ataxin-3 is required for the manifestation of symptoms in SCA3: *in vivo* evidence. *J. Neurosci.*, **27**, 7418–7428.
27. Boy, J., Schmidt, T., Wolburg, H., Mack, A., Nuber, S., Bottcher, M., Schmitt, I., Holzmann, C., Zimmermann, F., Servadio, A. *et al.* (2009) Reversibility of symptoms in a conditional mouse model of spinocerebellar ataxia type 3. *Hum. Mol. Genet.*, **18**, 4282–4295.
28. Silva-Fernandes, A., Costa, M.D., Duarte-Silva, S., Oliveira, P., Botelho, C.M., Martins, L., Mariz, J.A., Ferreira, T., Ribeiro, F., Correia-Neves, M. *et al.* (2010) Motor uncoordination and neuropathology in a transgenic mouse model of Machado–Joseph disease lacking intranuclear inclusions and ataxin-3 cleavage products. *Neurobiol. Dis.*, **40**, 163–167.
29. Alves, S., Regulier, E., Nascimento-Ferreira, I., Hassig, R., Dufour, N., Koeppen, A., Carvalho, A.L., Simoes, S., de Lima, M.C., Brouillet, E. *et al.* (2008) Striatal and nigral pathology in a lentiviral rat model of Machado–Joseph disease. *Hum. Mol. Genet.*, **17**, 2071–2083.
30. Albertson, D.G. and Thomson, J.N. (1976) The pharynx of *Caenorhabditis elegans*. *Phil. Trans. R. Soc. Lond .B. Biol. Sci.*, **275**, 299–325.
31. White, J.G., Southgate, E., Thomson, J.N. and Brenner, S. (1976) The structure of the ventral nerve cord of *Caenorhabditis elegans*. *Phil. Trans. R. Soc. Lond. B. Biol. Sci.*, **275**, 327–348.
32. Brignull, H.R., Moore, F.E., Tang, S.J. and Morimoto, R.I. (2006) Polyglutamine proteins at the pathogenic threshold display neuron-specific aggregation in a pan-neuronal *Caenorhabditis elegans* model. *J. Neurosci.*, **26**, 7597–7606.
33. Faber, P.W., Alter, J.R., MacDonald, M.E. and Hart, A.C. (1999) Polyglutamine-mediated dysfunction and apoptotic death of a *Caenorhabditis elegans* sensory neuron. *Proc. Natl Acad. Sci. USA*, **96**, 179–184.
34. Satyal, S.H., Schmidt, E., Kitagawa, K., Sondheimer, N., Lindquist, S., Kramer, J.M. and Morimoto, R.I. (2000) Polyglutamine aggregates alter protein folding homeostasis in *Caenorhabditis elegans*. *Proc. Natl Acad. Sci. USA*, **97**, 5750–5755.
35. Parker, J.A., Connolly, J.B., Wellington, C., Hayden, M., Dausset, J. and Neri, C. (2001) Expanded polyglutamines in *Caenorhabditis elegans* cause axonal abnormalities and severe dysfunction of PLM mechanosensory neurons without cell death. *Proc. Natl Acad. Sci. USA*, **98**, 13318–13323.
36. Morley, J.F., Brignull, H.R., Weyers, J.J. and Morimoto, R.I. (2002) The threshold for polyglutamine-expansion protein aggregation and cellular toxicity is dynamic and influenced by aging in *Caenorhabditis elegans*. *Proc. Natl Acad. Sci. USA*, **99**, 10417–10422.
37. Altun-Gultekin, Z., Andachi, Y., Tsalik, E.L., Pilgrim, D., Kohara, Y. and Hobert, O. (2001) A regulatory cascade of three homeobox genes, ceh-10, ttx-3 and ceh-23, controls cell fate specification of a defined interneuron class in *C. elegans*. *Development*, **128**, 1951–1969.
38. Berke, S.J., Schmied, F.A., Brunt, E.R., Ellerby, L.M. and Paulson, H.L. (2004) Caspase-mediated proteolysis of the polyglutamine disease protein ataxin-3. *J. Neurochem.*, **89**, 908–918.
39. Colomer Gould, V.F., Goti, D., Pearce, D., Gonzalez, G.A., Gao, H., Bermudez de Leon, M., Jenkins, N.A., Copeland, N.G., Ross, C.A. and Brown, D.R. (2007) A mutant ataxin-3 fragment results from processing at a site N-terminal to amino acid 190 in brain of Machado–Joseph disease-like transgenic mice. *Neurobiol. Dis.*, **27**, 362–369.
40. Haacke, A., Hartl, F.U. and Breuer, P. (2007) Calpain inhibition is sufficient to suppress aggregation of polyglutamine-expanded ataxin-3. *J. Biol. Chem.*, **282**, 18851–18856.
41. Haacke, A., Broadley, S.A., Boteva, R., Tzvetkov, N., Hartl, F.U. and Breuer, P. (2006) Proteolytic cleavage of polyglutamine-expanded ataxin-3 is critical for aggregation and sequestration of non-expanded ataxin-3. *Hum. Mol. Genet.*, **15**, 555–568.
42. Teixeira-Castro, A., Dias, N., Rodrigues, P., Oliveira, J.O., Rodrigues, N.F., Maciel, P. and Vilaça, J.L. (2011) An image processing application for quantification of protein aggregates in *Caenorhabditis elegans*. *In 5th International Conference on Practical Applications of Computational Biology & Bioinformatics. Advances in Soft Computing*. Springer, Vol. 93, pp. 31–38.
43. Garcia, S.M., Casanueva, M.O., Silva, M.C., Amaral, M.D. and Morimoto, R.I. (2007) Neuronal signaling modulates protein homeostasis in *Caenorhabditis elegans* post-synaptic muscle cells. *Genes Dev.*, **21**, 3006–3016.
44. Gidalevitz, T., Ben-Zvi, A., Ho, K.H., Brignull, H.R. and Morimoto, R.I. (2006) Progressive disruption of cellular protein folding in models of polyglutamine diseases. *Science*, **311**, 1471–1474.
45. Bargmann, C.I., Hartwieg, E. and Horvitz, H.R. (1993) Odorant-selective genes and neurons mediate olfaction in *C. elegans*. *Cell*, **74**, 515–527.
46. Kimura, K.D., Tissenbaum, H.A., Liu, Y. and Ruvkun, G. (1997) daf-2, an insulin receptor-like gene that regulates longevity and diapause in *Caenorhabditis elegans*. *Science*, **277**, 942–946.
47. Arantes-Oliveira, N., Berman, J.R. and Kenyon, C. (2003) Healthy animals with extreme longevity. *Science*, **302**, 611.
48. Lin, K., Dorman, J.B., Rodan, A. and Kenyon, C. (1997) daf-16: An HNF-3/forkhead family member that can function to double the life-span of *Caenorhabditis elegans*. *Science*, **278**, 1319–1322.
49. Ogg, S., Paradis, S., Gottlieb, S., Patterson, G.I., Lee, L., Tissenbaum, H.A. and Ruvkun, G. (1997) The Fork head transcription factor DAF-16 transduces insulin-like metabolic and longevity signals in *C. elegans*. *Nature*, **389**, 994–999.
50. Evason, K., Collins, J.J., Huang, C., Hughes, S. and Kornfeld, K. (2008) Valproic acid extends *Caenorhabditis elegans* lifespan. *Aging Cell*, **7**, 305–317.

51. Hajdu-Cronin, Y.M., Chen, W.J. and Sternberg, P.W. (2004) The L-type cyclin CYL-1 and the heat-shock-factor HSF-1 are required for heat-shock-induced protein expression in *Caenorhabditis elegans*. *Genetics*, **168**, 1937–1949.
52. Jung, J., Xu, K., Lessing, D. and Bonini, N.M. (2009) Preventing Ataxin-3 protein cleavage mitigates degeneration in a *Drosophila* model of SCA3. *Hum. Mol. Genet.*, **18**, 4843–4852.
53. Ikeda, H., Yamaguchi, M., Sugai, S., Aze, Y., Narumiya, S. and Kakizuka, A. (1996) Expanded polyglutamine in the Machado–Joseph disease protein induces cell death *in vitro* and *in vivo*. *Nat. Genet.*, **13**, 196–202.
54. Boeddrich, A., Gaumer, S., Haacke, A., Tzvetkov, N., Albrecht, M., Evert, B.O., Muller, E.C., Lurz, R., Breuer, P., Schugardt, N. *et al.* (2006) An arginine/lysine-rich motif is crucial for VCP/p97-mediated modulation of ataxin-3 fibrillogenesis. *EMBO J.*, **25**, 1547–1558.
55. Li, F., Macfarlan, T., Pittman, R.N. and Chakravarti, D. (2002) Ataxin-3 is a histone-binding protein with two independent transcriptional corepressor activities. *J. Biol. Chem.*, **277**, 45004–45012.
56. Zhong, X. and Pittman, R.N. (2006) Ataxin-3 binds VCP/p97 and regulates retrotranslocation of ERAD substrates. *Hum. Mol. Genet.*, **15**, 2409–2420.
57. Evert, B.O., Schelhaas, J., Fleischer, H., de Vos, R.A., Brunt, E.R., Stenzel, W., Klockgether, T. and Wullner, U. (2006) Neuronal intranuclear inclusions, dysregulation of cytokine expression and cell death in spinocerebellar ataxia type 3. *Clin. Neuropathol.*, **25**, 272–281.
58. Seidel, K., den Dunnen, W.F., Schultz, C., Paulson, H., Frank, S., de Vos, R.A., Brunt, E.R., Deller, T., Kampinga, H.H. and Rub, U. (2010) Axonal inclusions in spinocerebellar ataxia type 3. *Acta Neuropathol*, **120**, 449–460.
59. Rodrigues, A.J., do Carmo Costa, M., Silva, T.L., Ferreira, D., Bajanca, F., Logarinho, E. and Maciel, P. (2010) Absence of ataxin-3 leads to cytoskeletal disorganization and increased cell death. *Biochim. Biophys. Acta*, **1803**, 1154–1163.
60. Mazzucchelli, S., De Palma, A., Riva, M., D'Urzo, A., Pozzi, C., Pastori, V., Comelli, F., Fusi, P., Vanoni, M., Tortora, P. *et al.* (2009) Proteomic and biochemical analyses unveil tight interaction of ataxin-3 with tubulin. *Int. J. Biochem. Cell Biol.*, **41**, 2485–2492.
61. Gidalevitz, T., Krupinski, T., Garcia, S. and Morimoto, R.I. (2009) Destabilizing protein polymorphisms in the genetic background direct phenotypic expression of mutant SOD1 toxicity. *PLoS Genet.*, **5**, e1000399.
62. Subramaniam, S., Sixt, K.M., Barrow, R. and Snyder, S.H. (2009) Rhes, a striatal specific protein, mediates mutant-huntingtin cytotoxicity. *Science*, **324**, 1327–1330.
63. Dickstein, D.L., Kabaso, D., Rocher, A.B., Luebke, J.I., Wearne, S.L. and Hof, P.R. (2007) Changes in the structural complexity of the aged brain. *Aging Cell*, **6**, 275–284.
64. Cohen, E., Paulsson, J.F., Blinder, P., Burstyn-Cohen, T., Du, D., Estepa, G., Adame, A., Pham, H.M., Holzenberger, M., Kelly, J.W. *et al.* (2009) Reduced IGF-1 signaling delays age-associated proteotoxicity in mice. *Cell*, **139**, 1157–1169.
65. Outeiro, T.F., Kontopoulos, E., Altmann, S.M., Kufareva, I., Strathearn, K.E., Amore, A.M., Volk, C.B., Maxwell, M.M., Rochet, J.C., McLean, P.J. *et al.* (2007) Sirtuin 2 inhibitors rescue alpha-synuclein-mediated toxicity in models of Parkinson's disease. *Science*, **317**, 516–519.
66. van Ham, T.J., Thijssen, K.L., Breitling, R., Hofstra, R.M., Plasterk, R.H. and Nollen, E.A. (2008) *C. elegans* model identifies genetic modifiers of alpha-synuclein inclusion formation during aging. *PLoS Genet.*, **4**, e1000027.
67. Parker, J.A., Arango, M., Abderrahmane, S., Lambert, E., Tourette, C., Catoire, H. and Neri, C. (2005) Resveratrol rescues mutant polyglutamine cytotoxicity in nematode and mammalian neurons. *Nat. Genet.*, **37**, 349–350.
68. Cohen, E., Du, D., Joyce, D., Kapernick, E.A., Volovik, Y., Kelly, J.W. and Dillin, A. (2010) Temporal requirements of insulin/IGF-1 signaling for proteotoxicity protection. *Aging Cell*, **9**, 126–134.
69. Chai, Y., Koppenhafer, S.L., Bonini, N.M. and Paulson, H.L. (1999) Analysis of the role of heat shock protein (Hsp) molecular chaperones in polyglutamine disease. *J. Neurosci.*, **19**, 10338–10347.
70. Williams, A.J., Knutson, T.M., Colomer Gould, V.F. and Paulson, H.L. (2009) *In vivo* suppression of polyglutamine neurotoxicity by C-terminus of Hsp70-interacting protein (CHIP) supports an aggregation model of pathogenesis. *Neurobiol. Dis.*, **33**, 342–353.
71. Brenner, S. (1974) The genetics of *Caenorhabditis elegans*. *Genetics*, **77**, 71–94.
72. Brignull, H.R., Morley, J.F., Garcia, S.M. and Morimoto, R.I. (2006) Modeling polyglutamine pathogenesis in *C. elegans*. *Methods Enzymol.*, **412**, 256–282.
73. Lewis, J.A. and Fleming, J.T. (1995) Basic culture methods. *Methods Cell Biol.*, **48**, 3–29.
74. Phair, R.D. and Misteli, T. (2000) High mobility of proteins in the mammalian cell nucleus. *Nature*, **404**, 604–609.
75. Voisine, C., Varma, H., Walker, N., Bates, E.A., Stockwell, B.R. and Hart, A.C. (2007) Identification of potential therapeutic drugs for Huntington's disease using *Caenorhabditis elegans*. *PLoS One*, **2**, e504.